ELSEVIER

Marine Micropaleontology 45 (2002) 269–290

MARINE MICROPALEONTOLOGY

www.elsevier.com/locate/marmicro

Plio-Pleistocene magnetic polarity stratigraphies and diagenetic magnetite dissolution at ODP Leg 177 Sites (1089, 1091, 1093 and 1094)

J.E.T. Channell [a,*], J.S. Stoner [b,1]

[a] *Department of Geological Sciences, PO Box 112120, University of Florida, Gainesville, FL 32611, USA*
[b] *Department of Geology, University of California, Davis, CA 95616, USA*

Received 30 June 2000; received in revised form 19 November 2000; accepted 15 March 2001

Abstract

Magnetic polarity stratigraphies from ODP Leg 177 'high resolution' sites indicate Brunhes sedimentation rates in the 12–25 cm/kyr range, with a trend of decreasing sedimentation rates with increasing age. Magnetite is the principal remanence-carrying mineral. Downcore alteration of magnetite and authigenic growth of iron sulfides introduces a high coercivity diagenetic remanence carrier (pyrrhotite). The change in pore water sulfate with depth in the sediment tends to be in step with the decrease in magnetization intensity, indicating the link between sulfate reduction and magnetite dissolution. Shipboard pass-through magnetometer data are generally very noisy due to a combination of weak magnetization intensities, drilling-related core deformation, and the influence of authigenic iron sulfides. Post-cruise progressive demagnetization of discrete samples aids the magnetostratigraphic interpretation, as these measurements are less influenced by low magnetization intensities and drilling-related deformation. The magnetostratigraphic interpretations provide much-needed calibration for biostratigraphic events in the high latitude southern oceans. Apart from the ODP Hole 745B (Kerguelen Plateau), published Plio-Pleistocene magnetostratigraphies from ODP sites in the Southern Ocean are poorly constrained. For this reason, we compare interpolated ages of 11 radiolarian events and one diatom event that occur at Hole 745B and Leg 177 sites.

Keywords: Pliocene–Pleistocene; magnetostratigraphy; magnetite dissolution; South Atlantic

1. Introduction

The high sedimentation rate sites drilled in 1997/1998 during ODP Leg 177 (Fig. 1) were the Southern Ocean analog to sediment drifts drilled in the Iceland Basin during ODP Leg 162. Mean sedimentation rates in the Brunhes Chron at Sites 1089, 1091 and 1094 lie in the 12–15 cm/kyr range, similar to Leg 162 sites. Site 1093 has a mean Brunhes sedimentation rate of ~25 cm/kyr bolstered by increased biogenic (diatom) sedimentation at this site.

Magnetic polarity stratigraphy provides the ba-

[1] Present address: Institute of Arctic and Alpine Research, University of Colorado, Campus Box 450, Boulder, CO 80309, USA.

* Corresponding author. Tel.: +1-352-392-3658; Fax: +1-352-392-9294.

E-mail address: jetc@ufl.edu (J.E.T. Channell).

0377-8398/02/$ – see front matter
PII: S0377-8398(02)00032-4

sic time-frame on which high resolution chronostratigraphic tools (such as oxygen isotope stratigraphy and geomagnetic paleointensity stratigraphy) are superposed. Biostratigraphy (mainly diatom and radiolarian biostratigraphy at Sites 1089, 1091, 1093 and 1094) provides a means of checking the pattern fit of polarity zones to the geomagnetic polarity timescale (GPTS), and the resulting fit serves to further constrain the age of biostratigraphic events. At Sites 1089, 1091, 1093 and 1094, the biogenic component is dominated by diatoms. The weight percent of opal varies from a minimum at Site 1089 (10–20%) to a maximum at Site 1093 (~70%). The predominant lithology at Site 1089 is diatom- and mud-bearing nannofossil ooze; at Site 1094, mud-bearing diatom ooze; and at Sites 1091 and 1093, diatom-rich ooze.

The natural remanent magnetization (NRM) in ODP Leg 177 sediments is carried by magnetite but superimposed on this detrital remanent magnetization (DRM) is a secondary (diagenetic) chemical remanent magnetization (CRM) carrier with high coercivity and unblocking temperatures below 350°C. This is probably pyrrhotite (Fe_xS_{x+1}) associated with the ubiquitous 'pyrite' documented in shipboard core descriptions.

2. Methods and procedures

Aboard the *R/V Joides Resolution*, magnetic susceptibility is routinely measured on whole core sections prior to splitting, using the multi-sensor track (MST). After core splitting, the working halves are described and sampled, while the remanent magnetization of archive halves is measured using the shipboard pass-through magnetometer. In-line alternating field (AF) demagnetization allows core sections to be progressively demagnetized to a maximum peak field of 80 mT, however, during ODP Leg 177, we did not exceed peak fields of 25 mT. The reason for not using higher peak fields was two-fold. Firstly, we determined that the secondary magnetization imposed by the drill string was removed at peak fields of 10–15 mT. Secondly, and more importantly, further NRM demagnetization would have compromised the cores for later high resolution (u-channel) studies.

Modern standards in paleomagnetic research dictate that the NRM be stepwise demagnetized in order to determine the component content of the magnetization. Aboard ship, we demagnetized core sections to a maximum peak field of 20–25 mT, with up to five demagnetization steps. The number of demagnetization steps depended upon time available to maintain core-flow through the shipboard core laboratory. Although these peak fields were apparently sufficient to remove the drilling-induced magnetization, they generally removed no more than 50–60% of the NRM and therefore the component content of the NRM could not be assessed from shipboard measurements.

Complete demagnetization was carried out post-cruise on discrete (7 cm^3) samples collected from the working halves of core sections from at least one hole per site, at a rate of 1–2 per section. The discrete samples were used to 'ground-truth' the shipboard pass-through data by stepwise (15–20 steps) AF demagnetization up to peak fields of 60–100 mT. Component magnetization directions were determined by picking (by eye) the demagnetization range in which the 'characteristic' magnetization component is defined, and then applying the standard least squares method (Kirschvink, 1980) to calculate the component direction.

Samples from Site 1089 (only) were subjected to thermal demagnetization after AF demagnetization, in order to determine the blocking temperature spectrum of a high coercivity component which is not demagnetized at peak fields in the 80–100 mT range (Fig. 2). Samples for thermal demagnetization were removed from their plastic cases (after drying in field-free space), wrapped in aluminum foil, and then stepwise heated in 25°C or 50°C steps until the magnetization intensity fell below magnetometer noise level. Subsequent to AF demagnetization, some discrete (7 cm^3) samples were sub-sampled to provide the ~20 mg of sediment necessary to generate hysteresis loops using the alternating gradient force magnetometer (μMag). Hysteresis loops, and the resulting hysteresis ratios (Fig. 3), help to constrain magnetic mineralogy and grain size.

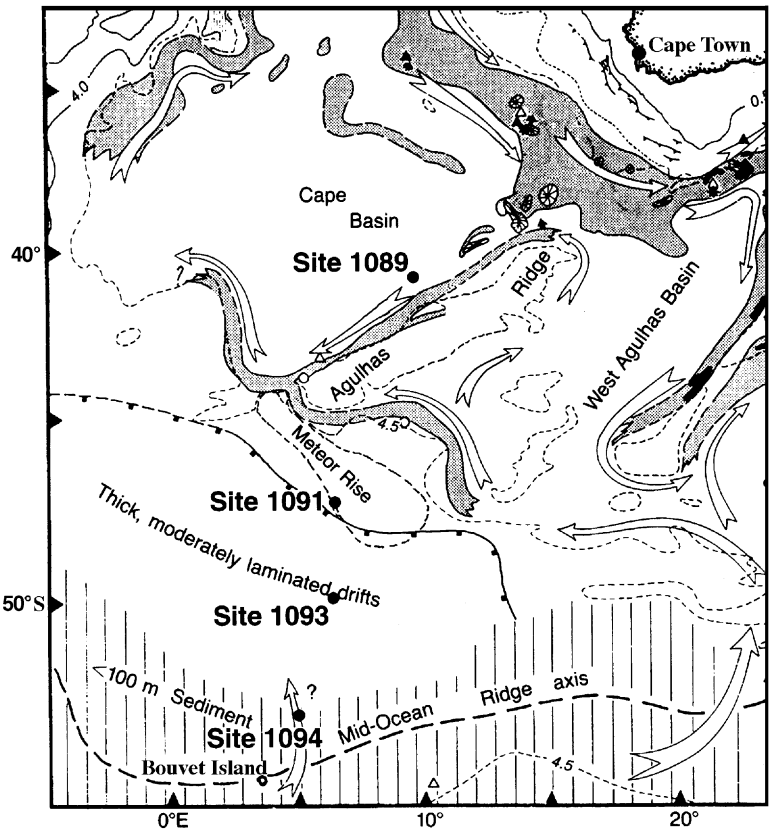

Fig. 1. Location of ODP Sites 1089, 1091, 1093 and 1094. Shading indicates circumbasin erosional zone separating Cape Basin and West Agulhas Basin. Arrows indicate bottom water flow. The line with square signature passing close to Site 1091 indicates the northern limit of thick laminated diatomaceous sediment (after Tucholke and Embley, 1984; Ciesielski et al., 1988; Gersonde et al., 1999).

3. Site 1089

Site 1089 (latitude 40°56.2′S, longitude 9°53.6′E) is located on the northern flank of the Agulhas Ridge in 4620 m water depth (Fig. 1). The motivation for drilling this site was partly derived from piston core RC11-83 (Charles et al., 1996) located closeby (latitude 41°36′S, longitude 9°48′E). For the last glacial cycle in RC11-83, Charles et al. (1996) argued that RC11-83 planktic ($\delta^{18}O$) and benthic ($\delta^{13}C$) isotopes provide proxy records of millennial scale climate change characteristic of the southern (e.g. δD Vostok Ice Core) and northern (e.g. $\delta^{18}O$ Greenland Summit Ice Core) hemispheres, respectively, and that southern hemispheric warming leads that of the north by 1500 yr. The main objective at Site 1089 was to extend the pioneering studies at RC11-83 back beyond the last glacial cycle.

Operations at Hole 1089A were plagued by numerous core liner failures, which resulted in core deformation that severely compromised the continuity of pass-through magnetometer measurements. Holes 1089B, 1089C and 1089D yielded considerably better quality cores due to improved core liner survival, however, synsedimentary deformation was recognized in these cores below ~90 m composite depth (mcd). The level at which synsedimentary slumping, microfaulting and inclined bedding were recognized was not uniform amongst the holes. For example, the first mention of evidence for slumping was recorded at

Site 1089

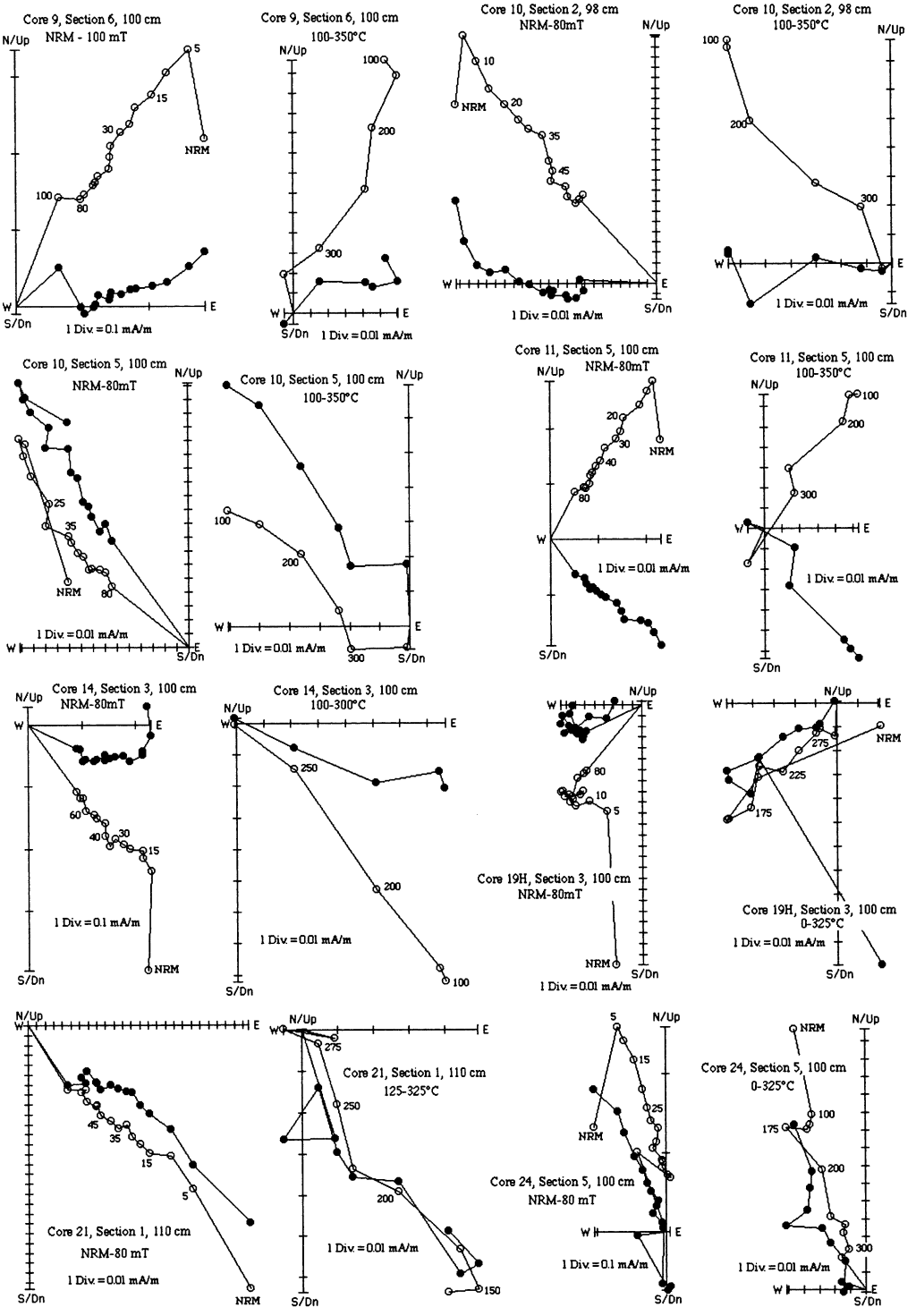
Core 9, Section 6, 100 cm
NRM - 100 mT
1 Div. = 0.1 mA/m
Core 9, Section 6, 100 cm
100-350°C
1 Div. = 0.01 mA/m
Core 10, Section 2, 98 cm
NRM-80mT
1 Div. = 0.01 mA/m
Core 10, Section 2, 98 cm
100-350°C
1 Div. = 0.01 mA/m
Core 10, Section 5, 100 cm
NRM-80mT
1 Div. = 0.01 mA/m
Core 10, Section 5, 100 cm
100-350°C
1 Div. = 0.01 mA/m
Core 11, Section 5, 100 cm
NRM-80mT
1 Div. = 0.01 mA/m
Core 11, Section 5, 100 cm
100-350°C
1 Div. = 0.01 mA/m
Core 14, Section 3, 100 cm
NRM-80mT
1 Div. = 0.1 mA/m
Core 14, Section 3, 100 cm
100-300°C
1 Div. = 0.01 mA/m
Core 19H, Section 3, 100 cm
NRM-80mT
1 Div. = 0.01 mA/m
Core 19H, Section 3, 100 cm
0-325°C
1 Div. = 0.01 mA/m
Core 21, Section 1, 110 cm
NRM-80 mT
1 Div. = 0.01 mA/m
Core 21, Section 1, 110 cm
125-325°C
1 Div. = 0.01 mA/m
Core 24, Section 5, 100 cm
NRM-80 mT
1 Div. = 0.1 mA/m
Core 24, Section 5, 100 cm
0-325°C
1 Div. = 0.01 mA/m
N/Up
S/Dn
NRM

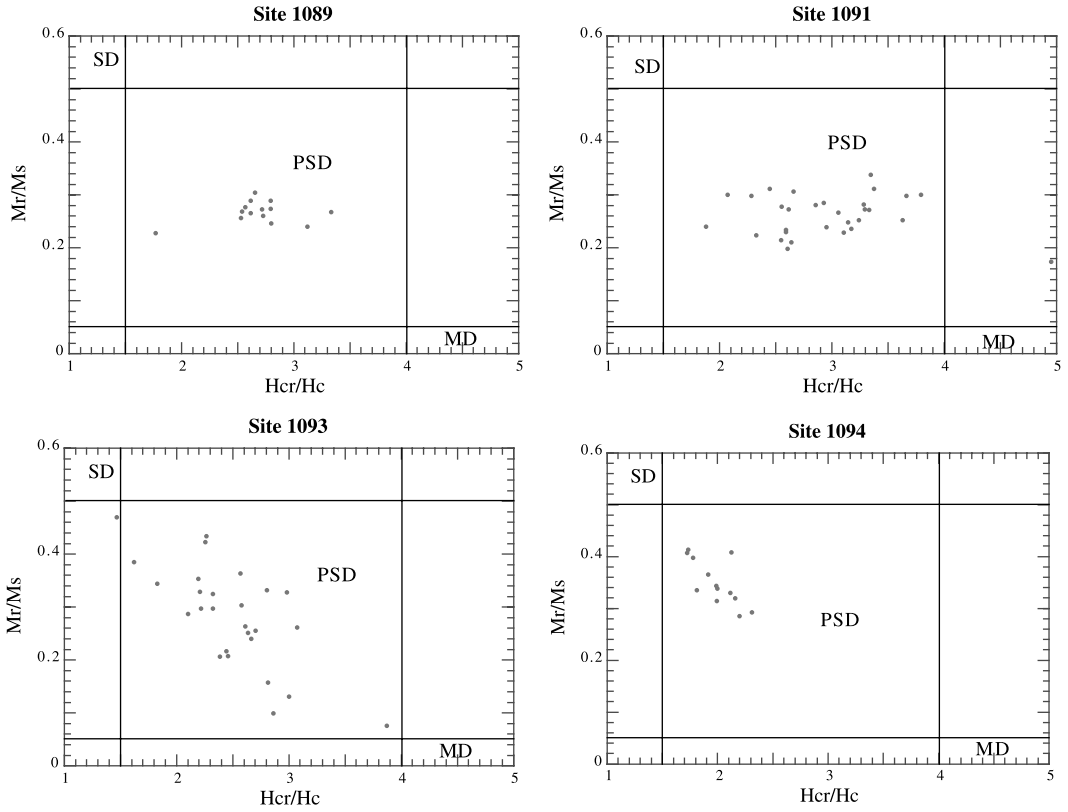

Fig. 3. Hysteresis ratios for Sites 1089, 1091, 1093 and 1094 plotted relative to the single domain (SD), pseudo-single domain (PSD) and multidomain (MD) fields for magnetite after Day et al. (1977).

149 mcd, 87 mcd and 106 mcd in Holes 1089B, 1089C and 1089D, respectively. This indicates that synsedimentary deformation was not always easy to recognize, and, undoubtedly, shipboard pass-through magnetometer measurements were compromised.

Approximately 200 discrete (7 cm^3) samples were collected from the least deformed intervals of Holes 1089A and 1089B core sections and therefore the problem of drilling-related deformation in Hole 1089A and synsedimentary deformation at all 1089 holes is partially ameliorated. The majority of discrete samples were collected from Hole 1089B which was not oriented using the tensor orientation tool, precluding declination correction.

Orthogonal projection of stepwise alternating field (AF) demagnetization of discrete samples from Site 1089 (Fig. 2) indicated that a steep downward overprint was removed at very low peak fields (5–10 mT). Prior to demagnetization, NRM intensities are generally in the 1–1.0 mA/m range. At least 15–20% of the NRM remains after demagnetization at peak fields of 80 mT indicating the presence of a high coercivity magnetization component. Thermal demagnetization of the

Fig. 2. Orthogonal projection of demagnetization data for Hole 1089B. Samples were first demagnetized using alternating fields (left) and the remaining remanence was then thermally demagnetized (right). Open and closed symbols indicate projection of vector end-points on the vertical and horizontal planes, respectively. Peak alternating fields are indicated in mT and temperatures in °C. The magnetization intensity associated with one division on the axes of each plot is indicated.

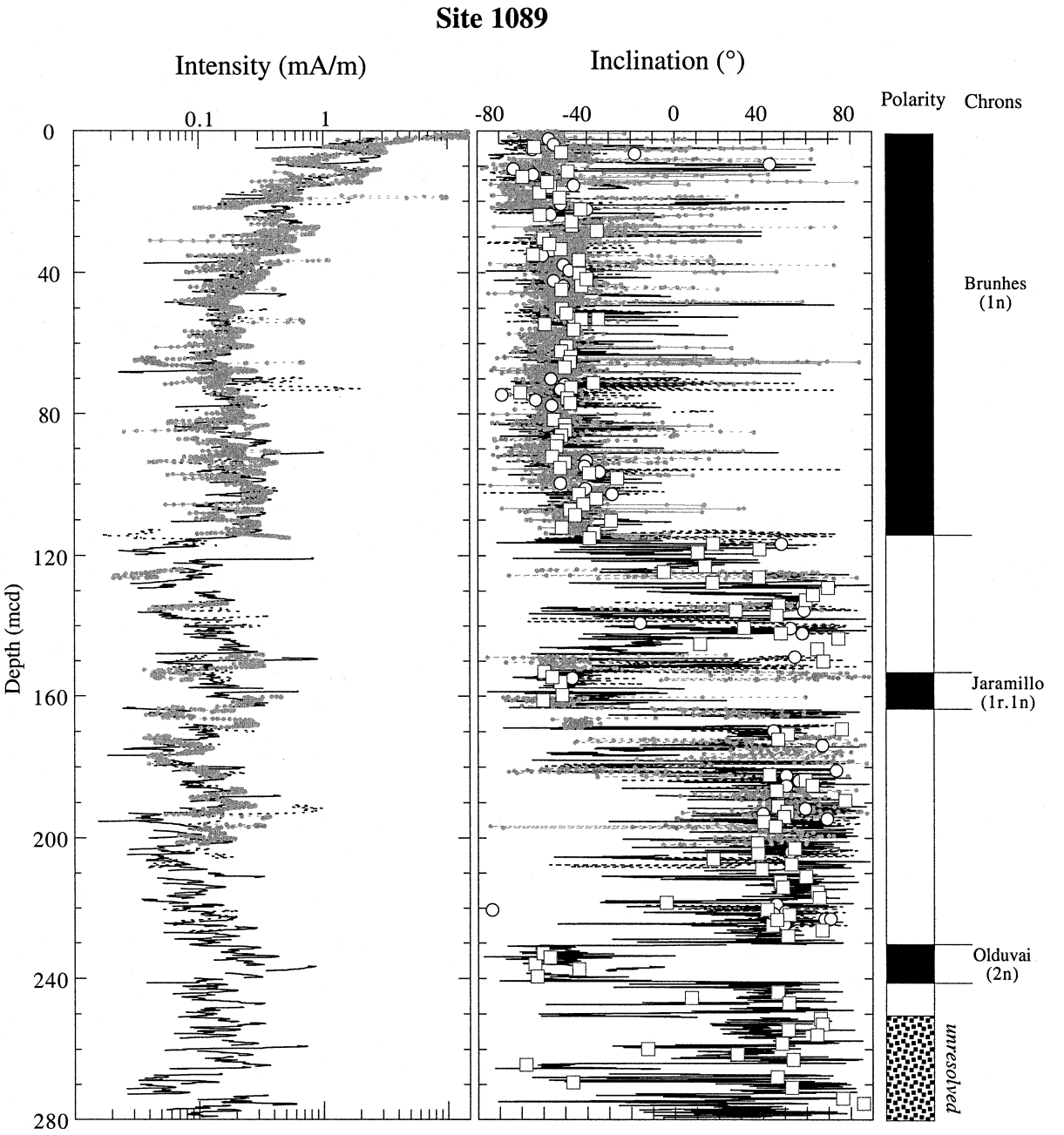

Fig. 4. Intensity and inclination of the magnetization direction after demagnetization at peak fields of 20 mT for Holes 1089A (black dashed line), 1089B (black continuous line), 1089C (gray dashed line with symbols) and 1089D (gray continuous line with symbols) measured with the shipboard pass-through magnetometer. Large open symbols indicate characteristic component inclinations for Hole 1089A (circles) and Hole 1089B (squares) calculated from stepwise alternating field demagnetization of discrete (7 cm^3) samples collected shipboard and measured on shore. Polarity interpretation is based in the inclination data. Meter levels of polarity zone boundaries are given in Table 1.

Table 1
Correlation of polarity zones to polarity chrons at Sites 1089, 1091, 1093 and 1094

Chron boundary	Age[a] (Ma)	Depth (mcd)	Est. uncertainty (m)	Based on
Site 1089				
Base Brunhes (base 1n)	0.78	116.3	±0.5	Hole B
Top Jaramillo (top 1r.1n)	0.99	151.6	±1	Hole B
Base Jaramillo (base 1r.1n)	1.07	163.3	±0.5	Holes B and C
Top Olduvai (top 2n)	1.77	230.7	±0.5	Hole B
Base Olduvai (base 2n)	1.95	240.8	±0.5	Hole B
Site 1091				
Base Brunhes (base 1n)	0.78	102.6	±0.3	Hole A
Top Jaramillo (top 1r.1n)	0.99	130.0	±2	Holes A,B,D
Base Jaramillo (base 1r.1n)	1.07	145.8	±0.5	Holes A and D
Top Olduvai (top 2n)	1.77	257.5	±0.5	Holes A and B
Base Olduvai (base 2n)	1.95	270.5	±0.5	Holes A and B
Top Gauss (top 2An)	2.58	311.0	±0.5	Hole A
Top Kaena and Mammoth?	3.04	323.0	±1	Hole A
Base Kaena and Mammoth?	3.33	327.0	±0.5	Hole A
Top Gilbert (top 2Ar)?	3.58	329.8	±0.3	Hole A
Site 1093				
Base Brunhes (base 1n)?	0.78	198.6	±2	Hole A
Top Gauss (top 2An)?	2.58	508.0	±2	Hole D
Top Gilbert (top 2Ar)?	3.58	577.0	±2	Hole D
Site 1094				
Base Brunhes (base 1n)	0.78	98.5	±0.5	Hole A
Top Jaramillo (top 1r.1n)	0.99	122.5	±1	Hole A
Base Jaramillo (base 1r.1n)	1.07	128.5	±1	Hole D
Cobb Mt.?	1.21	141.0	±1	Hole A

[a] Shackleton et al. (1990), Hilgen (1991a,b), and Cande and Kent (1995).

NRM remaining after AF demagnetization indicates that this high coercivity component has low unblocking temperature (<350°C). The only magnetic mineral that would have these characteristics is pyrrhotite (see Dekkers, 1988, 1989). Visual core descriptions indicate the ubiquitous presence of 'pyrite' (Shipboard Scientific Party, 1999a), and the pyrrhotite is probably associated with the observed pyrite. The chemical remanent magnetization (CRM) carried by pyrrhotite is a secondary magnetization produced during diagenesis, and is commonly formed at the expense of magnetite in organic-rich, reducing, diagenetic conditions (e.g. Kobayashi and Nomura, 1972; Canfield and Berner, 1987; Karlin, 1990; Channell and Hawthorne, 1990). In the case of Site 1089, we believe that the CRM is acquired during early diagenesis as it appears to record the same polarity as the low coercivity (magnetite) component (Fig. 2). Pore water sulfate decreases from 23 mM at 4 m below sea floor (mbsf) to near zero at 50 mbsf in Hole 1089A (Shipboard Scientific Party, 1999a). The reduction of pore water sulfate is mirrored by a decrease in magnetization intensity (Fig. 4) indicating that magnetite dissolution accompanies sulfate reduction. According to this model, sulfate is reduced to sulfide (by microbial activity), and the sulfide combines with the most reactive Fe available, which in this case is magnetite, to produce iron sulfides (mainly pyrite with associated pyrrhotite) (Canfield and Berner, 1987).

Magnetic hysteresis ratios lie in the pseudo-single domain (PSD) field of the Day et al. (1977) plot (Fig. 3). We note that the Site 1089 values do not lie on magnetite grain-size mixing line (between SD and MD). This trend and the wasp-waisted shape of the hysteresis loops indicates the presence of a high coercivity magnetization carrier (pyrrhotite) coexisting with a low coercivity carrier (magnetite) (see Channell and McCabe, 1994).

We base the magnetic polarity stratigraphy at Site 1089 on Hole 1089B magnetic inclination after demagnetization at 20 mT measured on the shipboard pass-through magnetometer, and the inclination of the magnetization component derived from discrete sample data (Fig. 4). The interpretation (Fig. 4, Table 1) is unresolved below 250 mcd where several cores (e.g. 1089B-27H) are characterized by steeply inclined bedding surfaces and microfaulting, indicating synsedimentary slumping.

4. Site 1091

Site 1091 (latitude 47°5.7′S, longitude 5°55.2′E) is located on the western flank of the Meteor Rise (Fig. 1) at a water depth of 4363 m. The site lies ~2°N of the present-day position of the Polar Front and is therefore an important site for reconstructing its movement and testing hypotheses related to changes in biological productivity and nutrient cycling. The lithology comprises diatom ooze in the glacial intervals and more calcareous diatom ooze, containing nannofossils and foraminifera, during interglacial periods. Intervals of intermittently laminated diatom mats occur between 91 and 231 mcd. The basal three cores of Hole 1091A (305–333 mcd) are more mud-rich than the section above. The composite section data, gamma-ray attenuation porosity evaluator (GRAPE), magnetic susceptibility, and color reflectance, indicate continuous overlap to 234 mcd with small gaps (~0.5 m) at ~8 mcd and ~79 mcd. Only Hole 1091A extends beyond 281 mcd.

Orthogonal projection of alternating field (AF) demagnetization data indicate that a single magnetization component can be resolved after removal of a low coercivity (drilling-related?) magnetization (Fig. 5). A large proportion of the NRM is lost after demagnetization at peak fields in the 60–80 mT range, and the median destructive field of the NRM is generally lower than at Site 1089. Natural remanent magnetization intensities (after demagnetization at peak fields of 25–30 mT) decrease in the uppermost 20–30 m (Fig. 6). NRM intensities vary about an average of 0.1 mA/m down to an abrupt increase to about 5 mA/m at 290 mcd, in 1091A-30H, associated with the abrupt change in lithology noted above.

The decrease in magnetization intensity in the top 20–30 m corresponds to a poorly documented, but apparently sharp, decrease in pore water sulfate. The microbial reduction of sulfate to sulfide results in the scavenging of reactive Fe (from magnetite in the absence of a more reactive Fe phase) and the growth of authigenic iron sulfides. The finer magnetite grains will be scavenged first due to their greater surface area to volume ratio, resulting in a loss of the more important (single domain and pseudo-single domain) remanence-carrying grains. Although pore water sulfate in the uppermost sediment is similar for Sites 1091 and 1089 (~28 mM), pore water sulfate is close to zero at 50 mbsf at Site 1089 but remains above 20 mM at 300 mbsf at Site 1091 (Shipboard Scientific Party, 1999b). It appears that microbially mitigated sulfate reduction is arrested at Site 1091, relative to Site 1089, possibly due to the lower availability of suitable organic matter at Site 1091.

Only the first 13 cores from Hole 1091A were oriented, therefore, the magnetic polarity stratigraphy was based on inclination data acquired shipboard using the pass-through magnetometer and shore-based study of discrete samples. The shipboard data are particularly noisy but the component inclinations determined from discrete samples help to resolve the magnetic stratigraphy (Fig. 6, Table 1).

5. Site 1093

Site 1093 (latitude 49°58.6′S, longitude 5°51.9′E, 3626 m water depth) was located north of Shona Ridge near the present-day position of the Polar Front but north of the present winter sea-ice limit (Fig. 1). The site is located in the circum-Antarctic opal belt and mean sedimentation rates are almost twice those at other Leg 177 sites, with particularly high sedimentation rates during interglacials. The site may record the deepest Matuyama–Brunhes boundary (MBB at ~200 mbsf) recovered in the pelagic realm, resulting in a mean Brunhes sedimentation rate of 25.6 cm/kyr.

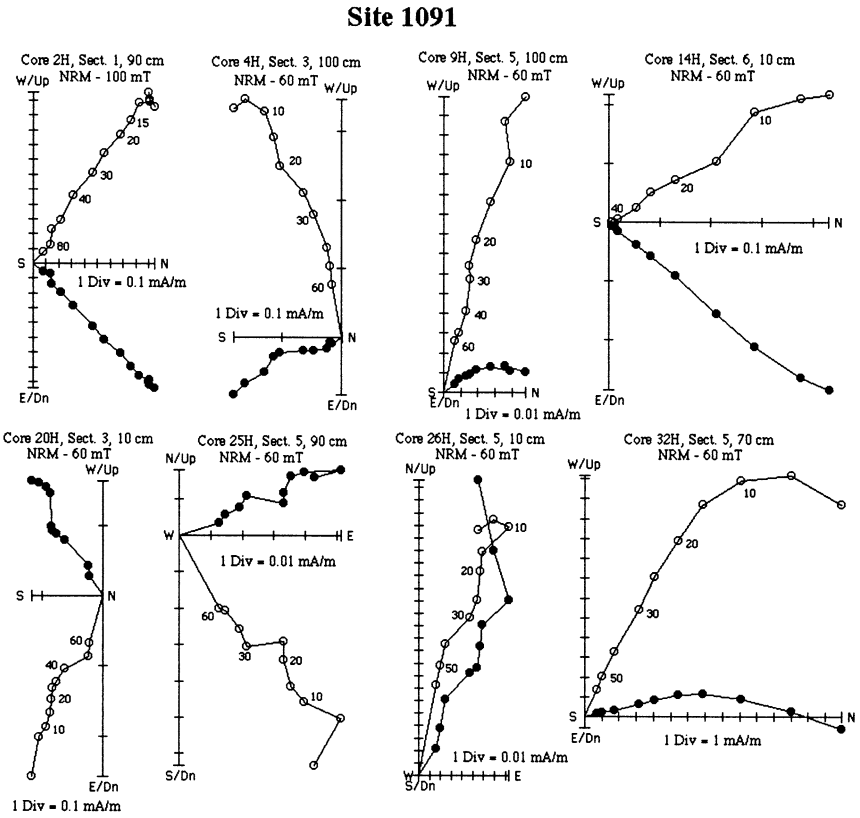

Fig. 5. Orthogonal projection of alternating field demagnetization data for Hole 1091A. Open and closed symbols indicate projection of vector end-points on the vertical and horizontal planes, respectively. Peak alternating fields are indicated in mT. The magnetization intensity associated with one division on the axes of each plot is indicated.

Orthogonal projections of alternating field (AF) demagnetization data indicate that a characteristic magnetization component can be resolved in some intervals (Fig. 7), although the magnetization intensities are very low, with about 10–25% of the NRM intensity remaining after demagnetization at peak fields of 60 mT. After demagnetization at peak fields of 25 mT, NRM intensities are generally about 0.1 mA/m (Fig. 8), only just over one order of magnitude greater than the noise level of the discrete sample cryogenic magnetometer at the University of Florida. Down-section changes in magnetization intensity (after AF demagnetization at peak fields of 25 mT) indicate an intensity drop in the uppermost 25 m (Fig. 8) which parallels the decrease in pore water sulfate. Magnetization intensities do not decrease systematically below this depth. Pore water sulfate is 28 mM close to the sediment surface, decreases steadily to 23 mM at 250 mbsf, and is in the 17–20 mM range at 400 mbsf (Shipboard Scientific Party, 1999c). As at Site 1091, the production of sulfide and resulting dissolution of magnetite is not sulfate-limited at Site 1093. The reduction of sulfate may be limited, below ~25 mbsf, by the availability of organic matter required by sulfate reducing microbial communities.

Although discrete sample data indicate that a characteristic magnetization component can be resolved (Fig. 7), the shipboard pass-through magnetometer inclination data are very noisy (Fig. 8). We attribute this to a combination of the following factors: (1) low intensity of NRM, (2) core liner 'contamination' by the core liner itself and by material entrained between sediment and core liner, (3) drilling-related sediment disturbance and

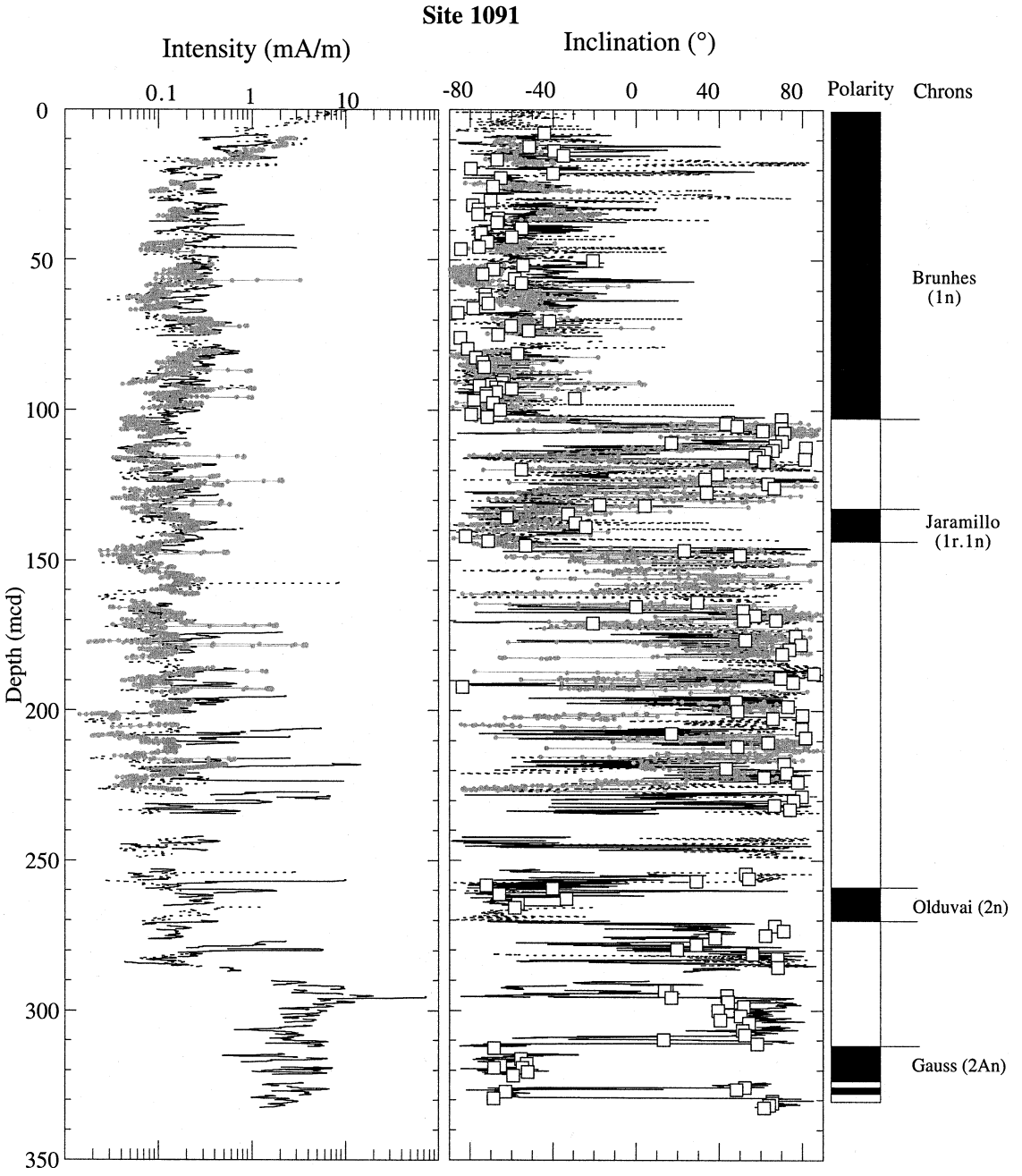

Fig. 6. Intensity and inclination of the magnetization direction after demagnetization at peak fields of 25 mT for Holes 1091A (black continuous line), 1091B (black dashed line), and 1091D (gray continuous line with symbols) measured with the shipboard pass-through magnetometer. Large open square symbols indicate characteristic component inclinations calculated from stepwise alternating field demagnetization of discrete (7 cm^3) samples collected shipboard and measured on shore. Polarity interpretation is based in the inclination data. Meter levels of polarity zone boundaries are given in Table 1.

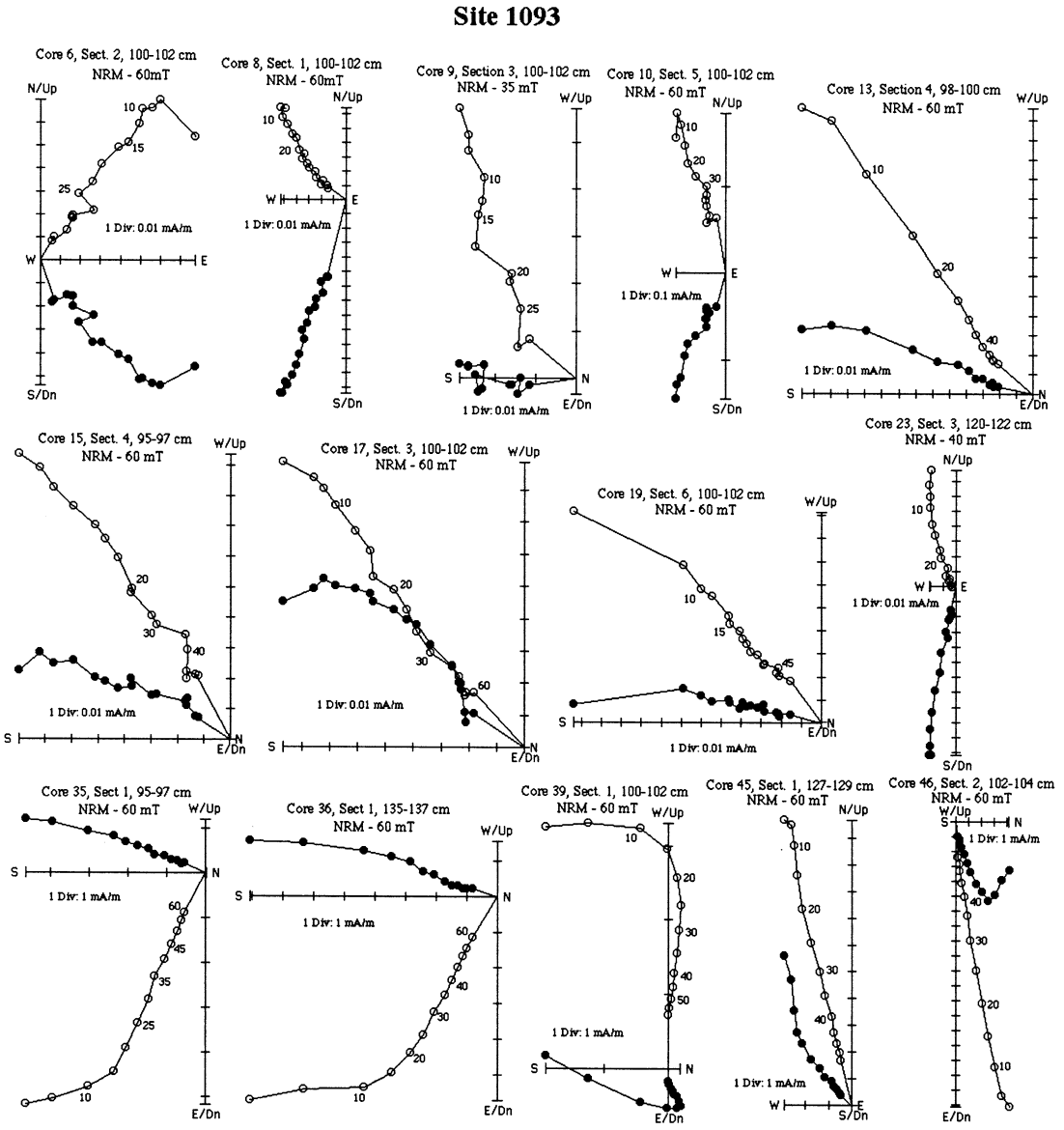

Fig. 7. Orthogonal projection of alternating field demagnetization data for Hole 1093A (top two rows) and 1093D (bottom row). Open and closed symbols indicate projection of vector end-points on the vertical and horizontal planes, respectively. Peak alternating fields are indicated in mT. The magnetization intensity associated with one division on the axes of each plot is indicated.

(4) prolonged diagenetic growth of iron sulfides which degrade the low intensity NRM. Discrete samples are less affected by these problems because they were measured on a more sensitive shore-based magnetometer, and were collected from the less deformed interior part of core sections. Even samples collected from diatom mats (e.g. 1093A-13H-4, 98–100 cm and 1093A-23H-3, 120–122 cm in Fig. 7) seem to be capable of recording a characteristic magnetization component. Magnetization intensities increase to about 1–10 mA/m for Cores 1093D-34X to 1093D-46X

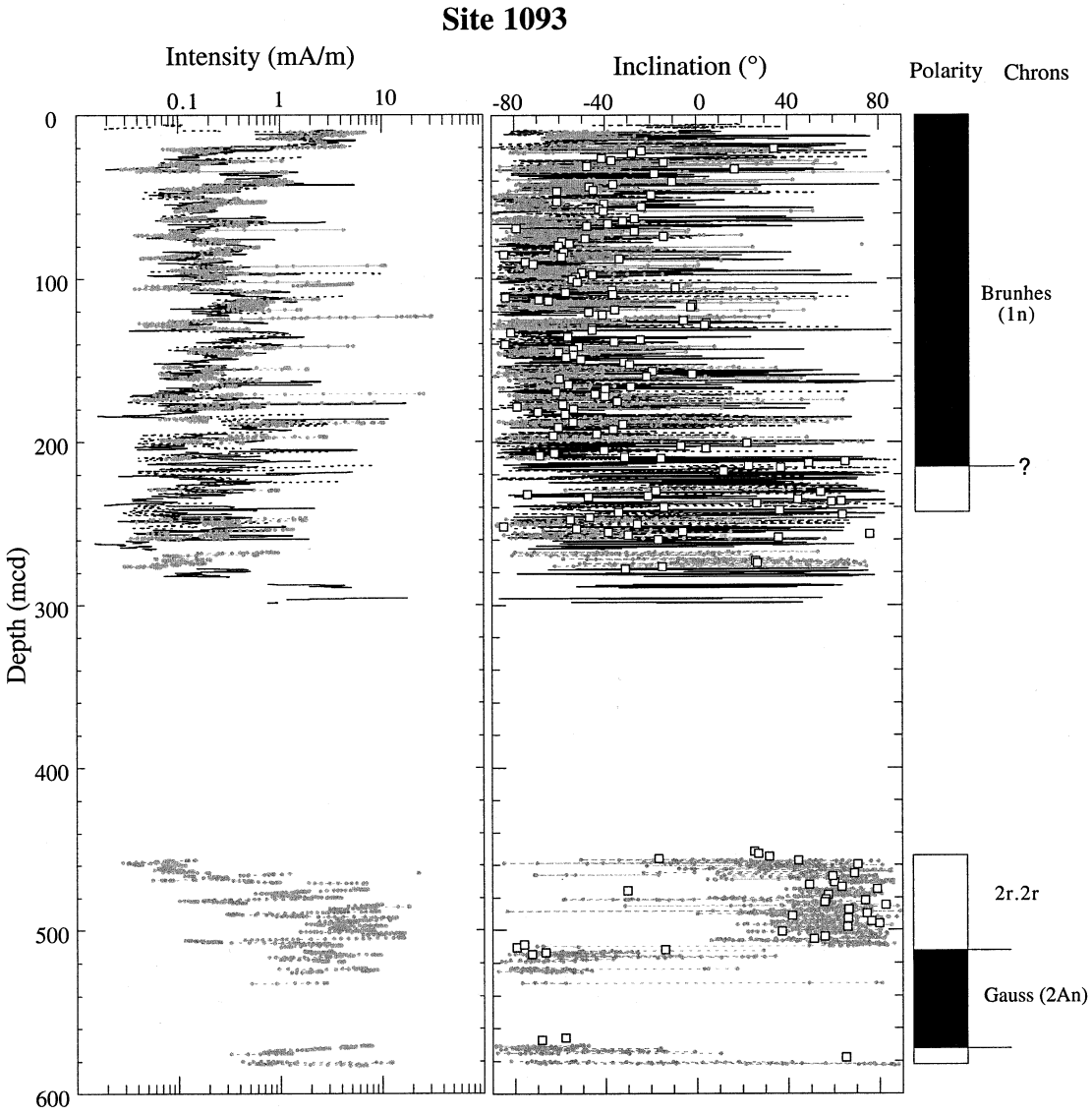

Fig. 8. Intensity and inclination of the magnetization direction after demagnetization at peak fields of 25 mT for Holes 1093A (black continuous line), 1093B (black dashed line), 1093C (gray continuous line with symbols) and 1093D (gray dashed line with symbols) measured with the shipboard pass-through magnetometer. Large open square symbols indicate component inclinations calculated from stepwise alternating field demagnetization of discrete (7 cm^3) samples collected shipboard and measured on shore. Polarity interpretation is based in the inclination data. Meter levels of polarity zone boundaries are given in Table 1.

(below 450 mcd, Fig. 8). We speculate that the increased mud content in lithologic Subunit 1B (461–590 mcd) accompanies increased detrital magnetite concentrations. The magnetic polarity stratigraphy is based mainly on discrete sample data due to the overall poor quality of the shipboard data (Fig. 8).

6. Site 1094

Site 1094 (latitude 53°10.8′S, longitude 5°7.8′E, water depth 2806 m) is the southernmost site drilled during ODP Leg 177 and lies south of the present-day Polar Front and ~2° north of the present-day average winter sea-ice limit. Sea-

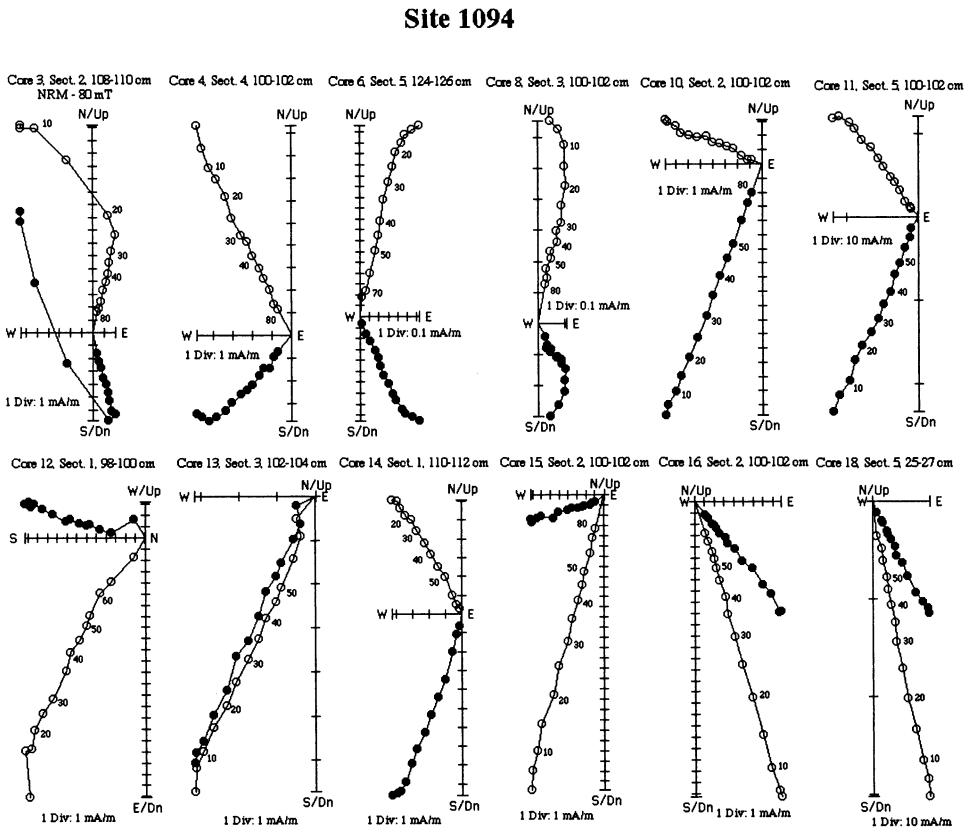

Fig. 9. Orthogonal projection of alternating field demagnetization data for Hole 1094A. Open and closed symbols indicate projection of vector end-points on the vertical and horizontal planes, respectively. Peak alternating fields are indicated in mT. The magnetization intensity associated with one division on the axes of each plot is indicated.

ice diagnostic diatoms indicate that the site was covered by sea-ice during the last glacial interval (Shipboard Scientific Party, 1999d). The lithology comprises olive gray to gray mud-bearing diatom ooze, with minor and varying amounts of foraminifera and nannofossils. Dispersed sand and gravel-sized volcanic ice rafted debris (IRD) are a minor but ubiquitous component. Most core-tops feature a gravel layer produced by cavings of IRD from the overlying section. IRD and sediment deformation resulting from it, as well as entrained IRD between the sediment and the core liner may account for some of the scatter in directional magnetic data. Multisensor track (MST) data, and hence the construction of the composite section, are also affected by drilling disturbance and by entrained IRD. A spliced sediment record was constructed to 121 mcd although there are seven ambiguous tie-points, and at least one known core gap between 1094A-7H and 1094A-8H which is not covered by the other holes drilled at the site (Shipboard Scientific Party, 1999d).

Orthogonal projections of alternating field demagnetization of discrete samples indicate that a characteristic magnetization component is well defined after demagnetization at peak fields of ~25 mT (Fig. 9). Here, the high coercivity magnetization component which is present at Sites 1089, 1091 and 1093 is largely absent. In contrast to the other sites, most of the NRM is lost after demagnetization in peak fields greater than 80 mT (Fig. 9). The magnetic hysteresis ratios for Site 1094 lie in the pseudo-single domain (PSD) field,

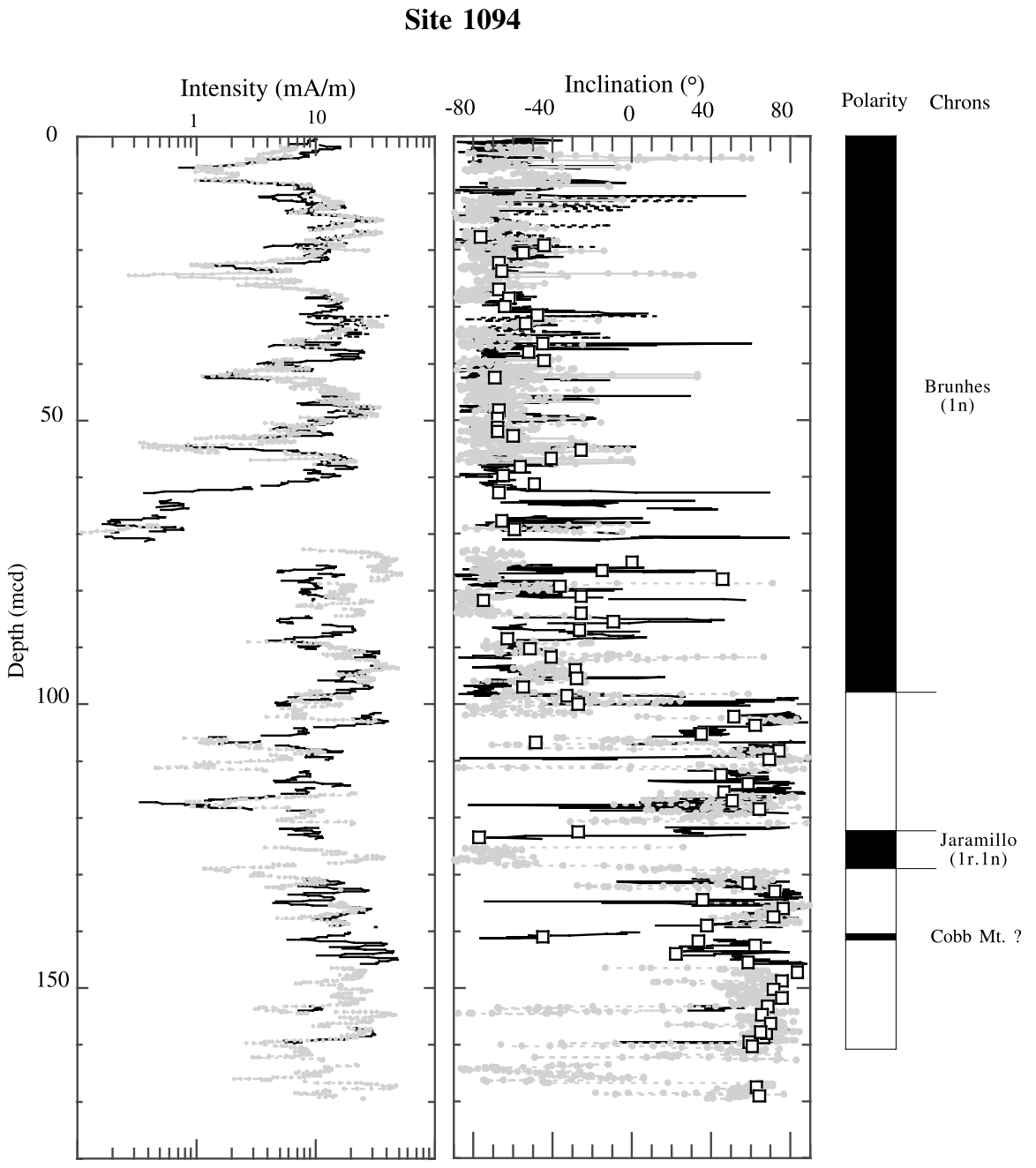

Fig. 10. Intensity and inclination of the magnetization direction after demagnetization at peak fields of 25 mT for Holes 1094A (black continuous line), 1094B (black dashed line), 1094C (gray continuous line with symbols) and 1094D (gray dashed line with symbols) measured with the shipboard pass-through magnetometer. Large open square symbols indicate component inclinations calculated from stepwise alternating field demagnetization of discrete (7 cm^3) samples collected shipboard and measured on shore. Polarity interpretation is based in the inclination data. Meter levels of polarity zone boundaries are given in Table 1.

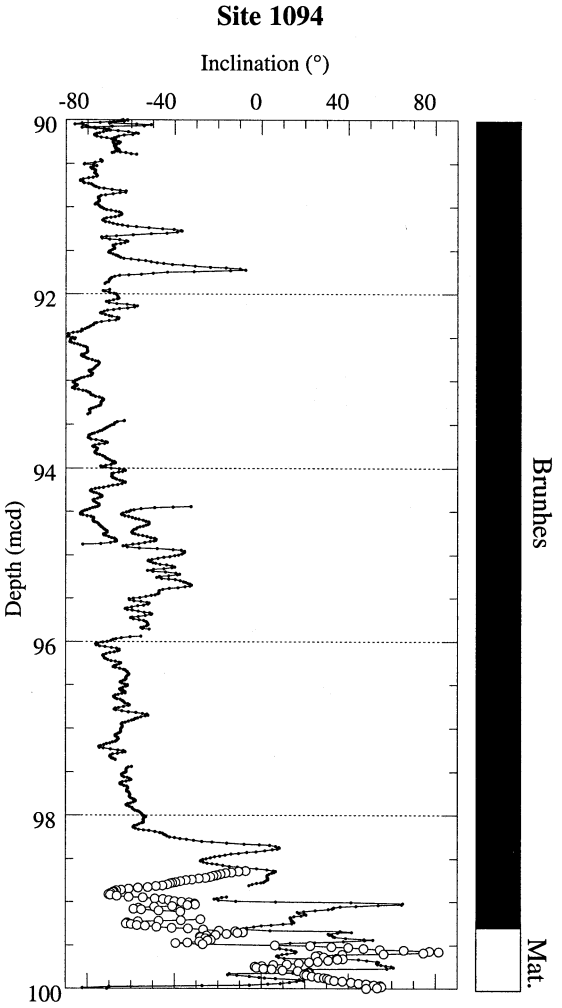

Fig. 11. Characteristic component inclinations determined from u-channel data in the 20–80 mT demagnetization range. Data from Cores 1094A-11H (small closed symbols) and 1094D-9H (large open symbols). Both cores indicate a Matuyama–Brunhes boundary in the 98–100 mcd interval.

and on a multidomain/single domain mixing line (Fig. 3).

In view of the sulfate reduction and magnetite dissolution inferred at the other sites, the lack of a high coercivity component (Fig. 9), and the lack of a progressive decrease in magnetization intensity (Fig. 10) imply that the process is not occurring at Site 1094. This is consistent with the observation that pore water sulfate concentrations at the base of the section at Site 1094 are indistinguishable from seawater values (Shipboard Scientific Party, 1999d). It remains a mystery (to us) as to why sulfate reduction (and subsequent magnetite dissolution) has not occurred at Site 1094. As speculated by the Shipboard Scientific Party (1999d), the process may be limited by the availability of reactive organic matter. In diatom-rich sediments much of the organic matter may be more refractory due to encasement in diatom tests, making it unavailable to sulfate reducing microbes.

At Site 1094, the polarity stratigraphy is based on the inclination record from shipboard data and component inclinations determined from discrete samples (Fig. 10). The position of the MBB at Site 1094 has also been determined from continuous 'u-channel' samples collected across the boundary. The change in component inclination at 99.0 mcd in Hole 1094A and at 99.5 mcd at Hole 1094D (Fig. 11) are slightly discrepant with respect to the estimate (98.5 mcd) from shipboard data and discrete sample data (Table 1, Fig. 10). Part of the discrepancy can be accounted for by imprecise hole-to-hole correlation at the site, where there are seven ambiguous tie-points in the composite section down to 121 mcd (Shipboard Scientific Party, 1999d). The generally noisy shipboard inclination data at this site (Fig. 10) are not attributed to low magnetization intensities or diagenetic growth of iron sulfides (as at other Leg 177 sites) but to drilling-related deformation of the cores.

7. Sedimentation rates and biomagnetostratigraphy

The polarity chron interpretation (Table 1) yields mean sedimentation rates within polarity zones (Fig. 12) with an overall tendency of increasing sedimentation rates over the last few million years. At Site 1093, the mean Brunhes sedimentation rate is 255 m/Myr (25.5 cm/kyr). We believe that this represents the thickest polarity zone of Brunhes age recovered in a pelagic marine environment. Mean Brunhes sedimentation rates at Sites 1089, 1091 and 1094 lie in the 13–15 cm/kyr range, comparable with sedimentation rates at drifts in the Iceland Basin (ODP Sites 983 and 984) (Channell and Lehman, 1999).

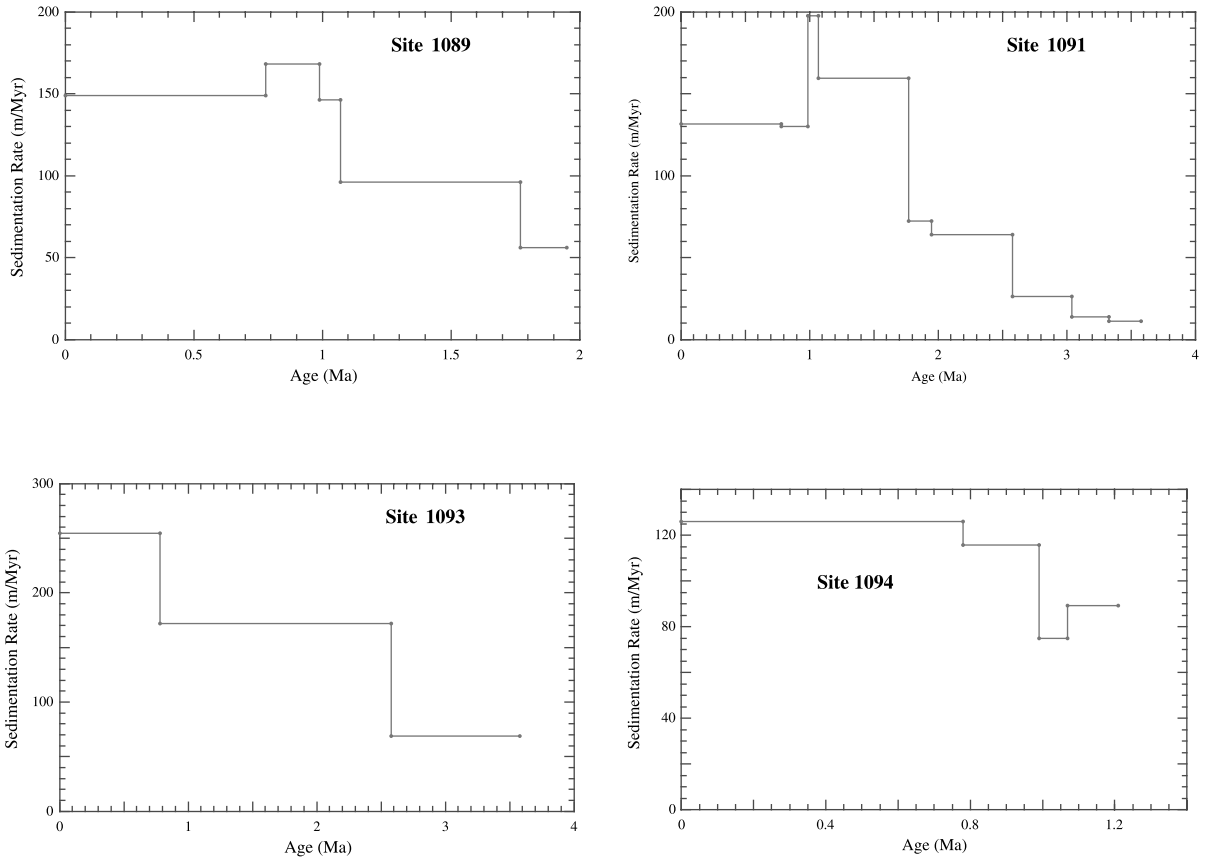

Fig. 12. Interval sedimentation rates for Site 1089, 1091, 1093, 1094 based on the magnetostratigraphic interpretations.

Unfortunately, the quality of the magnetic record at ODP Leg 177 high sedimentation rate sites is variable due to downcore magnetite dissolution, low initial magnetite concentrations leading to weak magnetization intensities, and drilling-related core deformation. Nonetheless, the high sedimentation rates at all sites (Fig. 12), and the more or less unambiguous identification of polarity chrons provides an opportunity to test the correlation of biostratigraphic markers and biozones to the GPTS.

For high southern latitude radiolaria, the work of Opdyke et al. (1966) and Hays and Opdyke (1967) were seminal contributions, placing late Neogene to Quaternary radiolarian events and biozones, for the first time, in a robust magnetostratigraphic frame. These publications were not only important in the history of biostratigraphy but also in the history of magnetostratigraphy, being among the first documentations of polarity reversals in sediments. Since the 1960s, workers in diatom and radiolarian biostratigraphy have been acutely aware of the importance of correlating their biostratigraphic observations to magnetostratigraphies. In the southern oceans, these correlations are particularly crucial due to the endemic nature and environmental sensitivity of siliceous biostratigraphic events. Keany (1979) studied the lower Pliocene radiolarian stratigraphy in 10 cores from close to the Antarctic Polar Front in the Indian and Pacific oceans. These authors adopted the polarity stratigraphy of Hays and Opdyke (1967) for one of these cores (E14-08), however, the polarity stratigraphy is not adequately documented for the other studied cores.

ODP Leg 113 in the Weddell Sea provided an

important advance in the study of middle Miocene to Recent radiolaria (Lazarus, 1990) and diatoms (Gersonde and Burckle, 1990), however, although the quality of the magnetic stratigraphy is excellent in the Paleocene to early Miocene (Spiess, 1990), the magnetostratigraphic data are very difficult to interpret for the younger part of the record. Thus from ODP Leg 113, direct correlation of radiolarian and diatom events to the GPTS is problematic for Plio-Pleistocene time.

For ODP Leg 114, quantitative diatom studies for the late Pliocene–Pleistocene interval at Hole 699A (Georgia Basin), Hole 701C (Islas Orcadas Rise) and Hole 704B (Meteor Rise) have been published (Fenner, 1991). Unfortunately, the Plio-Pleistocene magnetic stratigraphies at these holes are plagued by poor recovery and drilling disturbance. At Sites 701 and 704, the Brunhes/Matuyama magnetostratigraphies are ambiguous although the Gauss Chron is well defined (Hailwood and Clement, 1991a,b). At Hole 699A, the Olduvai Subchronozone is well defined but the boundaries of the Matuyama Chron cannot be defined with confidence (Hailwood and Clement, 1991c).

ODP Legs 119 and 120, off the Kerguelen Plateau, provided another opportunity to study high southern latitude diatoms (Baldauf and Barron, 1991; Harwood and Maruyama, 1992) and radiolaria (Caulet, 1991; Lazarus, 1992). For the most part, Plio-Pleistocene magnetic stratigraphies from ODP Legs 119 and 120 are uninterpretable (Keating and Sakai, 1991; Heider et al., 1992; Inokuchi and Heider, 1992). The exception is the Plio-Pleistocene magnetic stratigraphy from Hole 745B (Sakai and Keating, 1991) which can be interpreted without much ambiguity, allowing correlation of biostratigraphic events to the GPTS for sediments with sedimentation rates in the 3–5 cm/kyr range. From Hole 745B, semi-quantitative range charts for diatoms (Baldauf and Barron, 1991) and radiolaria (Caulet, 1991) are available.

Additional stratigraphic information, particularly for diatoms, is available from the numerous piston cores recovered by *RV Polarstern* in the Atlantic sector of the Southern Ocean (see Gersonde and Bárcena, 1998; Abelmann et al., 1990). Although these biostratigraphies are correlated to the GPTS, the primary magnetic stratigraphy does not appear in these papers and is not yet published (Gersonde, personal communication, 2000). Since the work of Opdyke et al. (1966), there have been few Plio-Pleistocene radiolarian studies in which the biostratigraphy is clearly matched to polarity stratigraphy. The works of Johnson et al. (1989) and Moore et al. (1993) are exceptions in that radiolarian events can be matched to an unambiguous magnetic stratigraphy, however, these studies are from the tropical Indian Ocean and the eastern equatorial Pacific (ODP Leg 138), not from the southern oceans.

In view of the paucity of direct (and documented) correlations of siliceous biostratigraphy to magnetic stratigraphy in the high and medium latitude Southern Ocean, the biomagnetostratigraphic results from ODP Leg 177 become highly significant (Sugiyama, personal communication; Zielinski and Gersonde, 2002). For purposes of comparison of ODP Leg 177 sites with Hole 745B (Kerguelen Plateau at 59.69°S, 86.85°E), we compare the stratigraphic position of one diatom datum (last occurrence (LO) of *Actinocylus ingens*) and 11 radiolarian events (Table 2), which represent a selection of the small number of bioevents that are documented both at the 'high resolution' Leg 177 sites and at Hole 745B. In Table 2, we also compare the timing of two radiolarian events: LO *Stylatractus universus* and first occurrence (FO) *Theocalyptra davisiana* (equivalent to *Cycladophora davisiana*), with their timing in the equatorial Pacific (Moore et al., 1993) and tropical Indian Ocean (Johnson et al., 1989).

The derived ages of bioevents in Table 2 are based on the assumption of constant sedimentation rates within polarity chrons. For Site 1089, oxygen isotope stratigraphy in the Brunhes Chron (Hodell et al., 2001) permits correlation of biostratigraphic data to ages based on marine isotope stages.

LO *Actinocylus ingens*: This diatom event marks the base of the *Thalassiosira lentignosa* zone of Harwood and Maruyama (1992) and Gersonde and Bárcena (1998). In these and other publications, the age of 0.62 Ma (0.66 Ma based on a revised MBB age of 0.78 Ma) for this event is adopted from Ciesielski (1983) and is based on

Table 2
Diatom and radiolarian events with interpolated ages

Event	Hole/site/core	Interval (m)	Age control 1 (Ma) or MIS	Depth control 1 (m)	Age control 2 (Ma)	Depth control 2 (m)	Age of event (Ma)
LO *Actinocylus ingens*	745B	24.0–33.5 mbsf	0	0	0.78	42.45 mbsf	0.44–0.62
LO *Actinocylus ingens*	1089	85.91–87.41 mcd	MIS 14				0.56
LO *Actinocylus ingens*	1091	80.88–82.38 mcd	0	0	0.78	102.65 mcd	0.62–0.63
LO *Actinocylus ingens*	1093	175.40–176.90 mcd	0	0	0.78	198.50 mcd	0.69–0.70
LO *Actinocylus ingens*	1094	89.73–91.23 mcd	0	0	0.78	98.20 mcd	0.71–0.72
LO *Pterocanium trilobum*	745B	15–16.5 mbsf	0	0	0.78	42.45 mbsf	0.28–0.30
LO *Pterocanium trilobum*	1091	117.34–118.09 mcd	0.78	102.65 mcd	0.99	130.0 mcd	0.89–0.90
LO *Pterocanium trilobum*	1093	238.21–238.38 mcd	0	0	0.78	198.50 mcd	0.94
LO *Stylatractus universus*	845–847						0.40–0.45
LO *Stylatractus universus*	VM34-53		MIS 11				0.40–0.42
LO *Stylatractus universus*	745B	16.5–18.0 mbsf	0	0	0.78	42.45 mbsf	0.30–0.33
LO *Stylatractus universus*	1089	62.06–62.76 mcd	MIS 11				0.41
LO *Stylatractus universus*	1089	62.06–62.76 mcd	0	0	0.78	116.30 mcd	0.42
LO *Stylatractus universus*	1091	54.41–55.16 mcd	0	0	0.78	102.65 mcd	0.41–0.42
LO *Stylatractus universus*	1093	131.39–131.43 mcd	0	0	0.78	198.50 mcd	0.52
LO *Stylatractus universus*	1094	72.04–72.39 mcd	0	0	0.78	98.20 mcd	0.57
LO *Anthocyrtella callopisma*	745B	33.5–34.0 mbsf	0	0	0.78	42.45 mbsf	0.62–0.63
LO *Anthocyrtella callopisma*	1089	80.42–80.61 mcd	MIS 13				0.51
FO *Microcalpis araneafera*	745B	41.5–43.0 mbsf	0	0	0.78	42.45 mbsf	0.76–0.79
FO *Microcalpis araneafera*	1089	166.54–167.99 mcd	0.99	151.60 mcd	1.07	163.30 mcd	1.09–1.10
FO *Microcalpis araneafera*	1091	177.41–177.43 mcd	0.99	130.00 mcd	1.07	145.80 mcd	1.23
FO *Microcalpis araneafera*	1093	294.08–294.50 mcd	0	0	0.78	198.50 mcd	1.16
FO *Microcalpis araneafera*	1094	139.64–140.18 mcd	0.99	122.50 mcd	1.07	128.50 mcd	1.11–1.23
LO *Desmospyris spongiosa*	745B	110.0–111.5 mbsf	1.95	93.5 mbsf	2.58	112.5 mbsf	2.50–2.54
LO *Desmospyris spongiosa*	1091	300.09–300.39 mcd	1.95	270.50 mcd	2.58	311.0 mcd	2.41
LO *Desmospyris spongiosa*	1093	499.22–499.97 mcd	0.78	198.50 mcd	2.58	508.0 mcd	2.53
LO *Antarctissa cylindrica*	745B	34.0–33.5 mbsf	0	0	0.78	42.45 mbsf	0.62
LO *Antarctissa cylindrica*	1091	102.70–104.09 mcd	0	0	0.78	102.65 mcd	0.78–0.79
LO *Antarctissa cylindrica*	1093	206.70–207.67 mcd	0	0	0.78	198.50 mcd	0.81
LO *Antarctissa cylindrica*	1094	96.50–96.69 mcd	0	0	0.78	98.20 mcd	0.77
LO *Cycladophora pliocenica*	745B	84.5–86.0 mbsf	1.07	54.6 mbsf	1.77	91.5 mbsf	1.65
LO *Cycladophora pliocenica*	1089	223.22–227.59 mcd	1.07	163.3 mcd	1.77	230.7 mcd	1.71
LO *Cycladophora pliocenica*	1091	232.84–234.34 mcd	1.07	145.80 mcd	1.77	257.5 mcd	1.62
LO *Pseudocubus vema*	745B	109.5–110.0 mbsf	1.95	93.5 mbsf	2.58	112.5 mbsf	2.48–2.50
LO *Pseudocubus vema*	1091	301.4–301.5 mcd	1.95	270.5 mcd	2.58	311.0 mcd	2.43
LO *Pseudocubus vema*	1093	488.9–489.3 mcd	0.78	198.5 mcd	2.58	508.0 mcd	2.45
FO *Theocalyptra davisiana*	844–847						2.74–2.76
FO *Theocalyptra davisiana*	MD81-369						2.42–2.44
FO *Theocalyptra davisiana*	VM29-40						2.46–2.54
FO *Cycladophora davisiana*	745B	114.5–116.0 mbsf	2.58	112.5 mbsf	3.04	123.5 mbsf	2.7
FO *Cycladophora davisiana*	1089	261.22–263.55 mcd	1.77	230.7 mcd	1.95	240.8 mcd	2.75
FO *Cycladophora davisiana*	1091	315.19–315.55 mcd	2.58	311.0 mcd	3.04	323.0 mcd	2.75
FO *Cycladophora davisiana*	1093	510.22–510.97 mcd	2.58	508 mcd	3.58	577 mcd	2.62
LO *Prunopyle titan*	745B	130.5–132.0 mbsf	3.33	128.5 mcd	3.58	133.0 mbsf	3.44–3.65
LO *Prunopyle titan*	1091	328.6–329.2 mcd	3.33	327.0 mcd	3.58	329.80 mbsf	3.47–3.52
LO *Prunopyle titan*	1093	571.12–571.20 mcd	2.58	508.0 mcd	3.58	577.00 mbsf	3.49
LO *Lychnocanium grande*	745B	164.4–165.9 mbsf	4.80	160.8 mbsf	4.89	167.9 mbsf	4.84–4.86
LO *Lychnocanoma grande*	1091	325.4–325.6 mcd	3.33	327.0 mcd	3.58	329.8 mcd	3.46
LO *Lychnocanoma grande*	1093	577.7–578.4 mcd	2.58	508.0 mcd	3.58	577.0 mcd	3.59

Table legend next page.

Islas Orcados piston core 11-70 from the SE Atlantic at 55°9′S, 9°59′E. The precision of this age estimate is limited by the low mean Brunhes sedimentation rate (1.7 cm/kyr) in this core. At Hole 745B, the potential resolution is improved as the MBB lies at 42.3–42.6 mbsf, however, only core-catcher samples were studied for diatoms in the Pleistocene and the event is therefore not precisely known within the 24.0–33.5 mbsf interval (Baldauf and Barron, 1991). At Site 1089, the LO *Actinocylus ingens* can be correlated to marine isotope stage (MIS) 14, yielding an age of 0.56 Ma. Assuming constant sedimentation rate within the Brunhes Chron, the age of the LO *A. ingens* at Sites 1089, 1091, 1093 and 1094 is constrained to the 0.6258–0.72 Ma range (Table 2).

The LO *Pterocanium trilobum* at Hole 745B (Caulet, 1991) is located in the younger part of the Brunhes Chron whereas it occurs prior to the MBB at Leg 177 sites (Table 2).

The LO *Stylatractus universus* is one of the most widely documented radiolarian events. It has been correlated to the MIS 11/12 transition (~420 ka) over a wide area of the Atlantic and Pacific oceans (Hays and Shackleton, 1976; Morley and Shackleton, 1978). The age of this event at Leg 177 sites is consistent with this estimate (Table 2). At Site 1089, the event lies in MIS 11 at 0.41 Ma. The event appears to have the same age in eastern equatorial Pacific at ODP Sites 845–847 (Moore et al., 1993) and in Core VM34-53 from the tropical Indian Ocean (Johnson et al., 1989).

The LO *Anthocyrtella callopisma* is located in the middle part of the Brunhes Chronozone at Hole 745B. At Site 1089, it correlates to MIS 13 at 0.51 Ma.

The FO *Microcalpis araneafera* occurs close to the MBB at Hole 745B, but is significantly older (close to the onset of the Jaramillo Subchron) at Leg 177 sites. The LO *Desmospyris spongiosa* and LO *Pseudocubus vema* occur close to the Matuyama–Gauss boundary both at Hole 745B and at Leg 177 sites.

LO *Antarctissa cylindrica*: Lazarus (1990) gives an age of 0.55 Ma for this event in the Weddell Sea. At Hole 745B, the event occurs in the 34.0–33.5 mbsf interval (Caulet, 1991). Assuming a constant sedimentation rate within the Brunhes Chron, this yields an age estimate of 0.62 Ma for the event (Table 2). In contrast, at the ODP Leg 177 sites, the event lies close to the MBB at 0.78–0.81 Ma (Table 2). This discrepancy may be due to different operational procedures for defining the last occurrence of a species which has sporadic occurrence at the end of its range. Sugiyama (personal communication) refers to the last common occurrence (LCO), rather than the LO referred to by Caulet (1991) at Hole 745B.

LO *Cycladophora pliocenica*: Lazarus (1990) gives an age of 1.6 Ma for this event and this age is very close to the ages determined from Hole 745B and Leg 177 sites (Table 2) assuming constant sedimentation rate between the base of the Jaramillo and the top of the Olduvai subchronozones.

FO *Cycladophora davisiana* (equivalent to *FO Theocalyptra davisiana*): Lazarus (1990) gave an age of 2.7 Ma for this event and this age is consistent with the ages determined both at Hole 745B and at Leg 177 sites (Table 2). It is also consistent with the FO *T. davisiana* at Sites 844–847 in the equatorial Pacific (Moore et al., 1993) but is older than the FO *T. davisiana* in the tropical Indian Ocean (MD81-369, VM29-40) where the event is younger than the Matuyama–Gauss boundary at 2.4–2.5 Ma (Table 2).

Ages of biostratigraphic events are determined assuming constant sedimentation rates within polarity chrons (between age control points 1 and 2), or from the marine oxygen isotope stage (MIS). The age control points are: top sediment (0 Ma), base of Brunhes Chron (0.78 Ma), top of Jaramillo (0.99 Ma), base of Jaramillo (1.07 Ma), top of Olduvai (1.77 Ma), base of Olduvai (1.95 Ma), base of Matuyama (2.58 Ma), top of Kaena (3.04 Ma), base of Mammoth (3.33 Ma), base of Gauss (3.58 Ma), top of Sidufjall (4.80 Ma) and base of Sidufjall (4.89 Ma). Data for Hole 745B (Kerguelen) from Caulet (1991) and Barron et al. (1991), for Leg 177 sites (1089, 1091, 1093 and 1094) from Sugiyama (personal communication) and Zielinski and Gersonde (2002), for VM34-53, MD81-369 and VM29-40 (tropical Indian Ocean) from Johnson et al. (1989), and Sites 844–847 (eastern equatorial Pacific) from Moore et al. (1993). Age of polarity chrons follow Shackleton et al. (1990) and Cande and Kent (1995). mcd, m composite depth, mbsf, m below sea floor.

Whereas the age of LO *Prunopyle titan* is consistent for the Hole 745B and Leg 177 sites, the LO *Lychnocanoma grande* (equivalent to *Lychnocanium grande*) is significantly younger (by over 1 Myr) at ODP Leg 177 relative to Hole 745B (Table 2). Inspection of the magnetic stratigraphy at Hole 745B (Sakai and Keating, 1991) indicates no obvious problem with the magnetostratigraphic interpretation in this interval. The event therefore appears to be diachronous between Kerguelen (Hole 745B) and Leg 177 sites.

8. Conclusions

A primary magnetization carried by magnetite can be isolated at Sites 1089, 1091, 1093 and 1094, however, dissolution of magnetite and growth of authigenic iron sulfides (including pyrrhotite) affects the fidelity of the magnetostratigraphic record at all sites. At Site 1089, the production of sulfide and consequent dissolution of magnetite appears to be sulfate-limited. Pore water concentration of sulfate decreases to zero at about 50 mbsf accompanied by a decrease in magnetic susceptibility and magnetization intensity. At the other sites, however, the concentration of sulfate in pore waters remains high to the base of the recovered section indicating that sulfate reduction is not a continuing process, even in the presence of a few percent organic carbon. We speculate that the organic carbon associated with the diatomaceous oozes may be too refractory to be utilized by sulfate reducing microbes. These conditions of arrested sulfate reduction may have saved the primary magnetization, and resulted in interpretable magnetic stratigraphies at Leg 177 sites.

A survey of published biomagnetostratigraphic data from the mid to high latitude southern oceans indicates that there are very few locations at which primary Plio-Pleistocene biomagnetostratigraphic correlations can be established due to poor quality magnetostratigraphies for the last 2–3 Myr for ODP Legs 113, 114, 119 and 120. The exception is Hole 745B from Leg 119 (Kerguelen Plateau). Here the Plio-Pleistocene magnetic stratigraphy is more easily interpreted allowing direct correlation of bioevents to the polarity timescale. A comparison of 12 siliceous bioevents (11 radiolarian events and one diatom event) between Hole 745B and ODP Leg 177 sites indicates synchroneity for all bioevents except for LO *Pterocanium trilobum*, FO *Microcalpis araneafera*, LO *Antarctissa cylindrica* and LO *Lychnocanoma grande*.

Acknowledgements

We thank K. Sugiyama, R. Gersonde, U. Bleil and C. Langereis for helpful comments on the manuscript. We thank K. Sugiyama, U. Zielinski and R. Gersonde for sharing their biostratigraphic data with us. Post-cruise magnetostratigraphic study of ODP Leg 177 sediments has been supported by a USSAC grant administered by the Ocean Drilling Program through Texas A&M University, and by the US National Science Foundation (OCE-97-11424).

References

Abelmann, A., Gersonde, R., Spiess, V., 1990. Pliocene paleoceanography in the Weddell Sea – siliceous microfossil evidence. In: Bleil, U., Thiede, J. (Eds.), Geological History of the Polar Oceans: Arctic versus Antarctic. Kluwer Academic Publishers, Dordrecht, pp. 729–759.

Baldauf, J.G., Barron, J.A., 1991. Diatom biostratigraphy: Kerguelen Plateau and Prydz Bay regions of the Southern Ocean. In: Barron, J., Larsen, B. et al. (Eds.), Proc. ODP Sci. Results 119. ODP, College Station, TX, pp. 547–598.

Barron, J.A., Baldauf, J.G., Barrera, E., Caulet, J.-P., Huber, B.T., Keating, B.H., Lazarus, D., Sakai, H., Thierstein, H.R., Wei, W., 1991. Biochronologic and magnetochronologic synthesis of Leg 119 sediments from the Kerguelen Plateau and Prydz Bay, Antarctica. In: Barron, J., Larsen, B. et al. (Eds.), Proc. ODP Sci. Results 119. ODP, College Station, TX, pp. 813–847.

Cande, S.C., Kent, D.V., 1995. Revised calibration of the geomagnetic polarity timescale for the Late Cretaceous and Cenozoic. J. Geophys. Res. 100, 6093–6095.

Canfield, D.E., Berner, R.A., 1987. Dissolution and pyritization of magnetite in anoxic marine sediments. Geochim. Cosmochim. Acta 51, 645–659.

Caulet, J.-P., 1991. Radiolarians from the Kerguelen Plateau, Leg 119. In: Barron, J., Larsen, B. et al. (Eds.), Proc. ODP Sci. Results. ODP, College Station, TX, pp. 513–546.

Channell, J.E.T., Hawthorne, T., 1990. Progressive dissolution

of titanomagnetites at ODP Site 653 (Tyrrhenian Sea). Earth Planet. Sci. Lett. 96, 469–480.

Channell, J.E.T., Lehman, B., 1999. Magnetic stratigraphy of North Atlantic Sites 980–984. In: Jansen, E., Raymo, M.E., Blum, P., Herbert, T. (Eds.), Proc. ODP Sci. Results 162. ODP, College Station, TX, pp. 113–130.

Channell, J.E.T., McCabe, C., 1994. Comparison of magnetic hysteresis parameters of unremagnetized and remagnetized limestones. J. Geophys. Res. 99, 4613–4623.

Charles, C.D., Lynch-Stieglitz, J., Ninnemann, U.S., Fairbanks, R.G., 1996. Climate connections between the hemispheres revealed by deep sea sediment core/ice core correlations. Earth Planet. Sci. Lett. 142, 19–27.

Ciesielski, P.F., 1983. The Neogene and Quaternary diatom biostratigraphy of subantarctic sediments, Deep Sea Drilling Project Leg 71. In: Ludwig, W.J., Krasheninnikov, V.A. et al. (Eds.), Init. Rep. DSDP 71. US Gov. Printing Office, Washington, DC, pp. 635–658.

Ciesielski, P.F., Kristoffersen, Y. et al., 1988. Proc. ODP Init. Rep. 114. ODP, College Station, TX.

Day, R., Fuller, M., Schmidt, V.A., 1977. Hysteresis properties of titanomagnetites: grain-size and compositional dependence. Phys. Earth Planet. Int. 13, 260–267.

Dekkers, M.J., 1988. Magnetic properties of natural pyrrhotite. Part I: Behaviour of initial susceptibility and saturation-magnetization related rock-magnetic parameters in a grain-size dependent framework. Phys. Earth Planet. Int. 52, 376–393.

Dekkers, M.J., 1989. Magnetic properties of natural pyrrhotite. II. High- and low-temperature behaviour of Jrs and TRM as a function of grain size. Phys. Earth Planet. Int. 57, 266–283.

Fenner, J.M., 1991. Late Pliocene–Quaternary quantitative diatom stratigraphy in the Atlantic sector of the Southern Ocean. In: Ciesielski, P.F., Kristoffersen, Y. et al. (Eds.), Proc. ODP Sci. Results 114. ODP, College Station, TX, pp. 97–121.

Gersonde, R., Bárcena, M.A., 1998. Revision of the upper Pliocene–Pleistocene diatom biostratigraphy for the northern belt of the southern ocean. Micropaleontology 44, 84–98.

Gersonde, R., Burckle, L.H., 1990. Neogene diatom biostratigraphy of ODP Leg 113, Weddell Sea (Antarctic Ocean). In: Barker, P.F., Kennett, J.P. et al. (Eds.), Proc. ODP Sci. Results 113. ODP, College Station, TX, pp. 761–789.

Gersonde, R., Hodell, D.A., Blum, P. et al., 1999. Proc. ODP Init. Rep. 177 [CD-ROM]. Available from: Ocean Drilling Program, Texas A&M University, College Station, TX.

Hailwood, E.A., Clement, B., 1991. Magnetostratigraphy of sediments from Sites 701 and 702. In: Ciesielski, P.F., Kristoffersen, Y. et al. (Eds.), Proc. ODP Sci. Results 114. ODP, College Station, TX, pp. 359–366.

Hailwood, E.A., Clement, B., 1991. Magnetostratigraphy of Sites 703 and 704, Meteor Rise, Southeastern South Atlantic. In: Ciesielski, P.F., Kristoffersen, Y. et al. (Eds.), Proc. ODP Sci. Results 114. ODP, College Station, TX, pp. 367–386.

Hailwood, E.A., Clement, B., 1991. Magnetostratigraphy of Sites 699 and 700, East Georgia Basin. In: Ciesielski, P.F., Kristoffersen, Y. et al. (Eds.), Proc. ODP Sci. Results 114. ODP, College Station, TX, pp. 337–357.

Harwood, D.M., Maruyama, T., 1992. Middle Eocene to Pleistocene diatom biostratigraphy of Southern Ocean sediments from the Kerguelen Plateau, Leg 120. In: Wise, S.W., Jr., Schlich, R. et al. (Eds.), Proc. ODP Sci. Results 120. ODP, College Station, TX, pp. 683–733.

Hays, J.D., Opdyke, N.D., 1967. Antarctic radiolaria, magnetic reversals, and climate change. Science 158, 1001–1011.

Hays, J.D., Shackleton, N.J., 1976. Globally synchronous extinction of the radiolarian *Stylatractus universus*. Geology 4, 649–652.

Heider, F., Leitner, B., Inokuchi, H., 1992. High southern latitude magnetostratigraphy and rock magnetic properties of sediments from Sites 747, 749 and 751. In: Wise, S.W., Jr., Schlich, R. et al. (Eds.), Proc. ODP Sci. Results 120. ODP, College Station, TX, pp. 225–245.

Hilgen, F.J., 1991a. Astronomical calibration of Gauss to Matuyama sapropels in the Mediterranean and implication for the geomagnetic polarity time scale. Earth Planet. Sci. Lett. 104, 226–244.

Hilgen, F.J., 1991b. Extension of the astronomically calibrated (polarity) time scale to the Miocene/Pliocene boundary. Earth Planet. Sci. Lett. 107, 349–368.

Hodell, D.A., Charles, C.D., Sierro, F.J., 2001. Late Pleistocene evolution of the ocean's carbonate system. Earth Planet. Sci. Lett. 192, 109–124.

Inokuchi, H., Heider, F., 1992. Magnetostratigraphy of sediments from Sites 748 and 750, Leg 120. In: Wise, S.W., Jr., Schlich, R. et al. (Eds.), Proc. ODP Sci. Results 120. ODP, College Station, TX, pp. 247–252.

Johnson, D.A., Schneider, D.A., Nigrini, C.A., Caulet, J.-P., Kent, D.V., 1989. Pliocene–Pleistocene radiolarian events and magnetostratigraphic calibrations for the tropical Indian Ocean. Mar. Micropaleontol. 14, 33–66.

Karlin, R., 1990. Magnetic diagenesis in marine sediments from the Oregon continental margin. J. Geophys. Res. 95, 4405–4419.

Keany, J., 1979. Early Pliocene radiolarian taxonomy and biostratigraphy in the Antarctic Region. Micropaleontology 25, 50–74.

Keating, B., Sakai, H., 1991. Magnetostratigraphic studies of sediments from Site 744, southern Kerguelen Plateau. In: Wise, S.W., Jr., Schlich, R. et al. (Eds.), Proc. ODP Sci. Results 120. ODP, College Station, TX, pp. 771–794.

Kirschvink, J.L., 1980. The least squares lines and plane analysis of paleomagnetic data. Geophys. J. R. Astron. Soc. 62, 699–718.

Kobayashi, K., Nomura, M., 1972. Iron sulfides in the sediment cores from the Sea of Japan and their geophysical implications. Earth Planet. Sci. Lett. 16, 200–208.

Lazarus, D., 1990. Middle Miocene to Recent radiolarians from the Weddell Sea, Antarctica, ODP Leg 113. In: Barker, P.F., Kennett, J.P. et al. (Eds.), Proc. ODP Sci. Results 113. ODP, College Station, TX, pp. 709–727.

Lazarus, D., 1992. Antarctic Neogene radiolarians from the Kerguelen Plateau, Legs 119 and 120. In: Wise, S.W., Jr., Schlich, R. et al. (Eds.), Proc. ODP Sci. Results 120. ODP, College Station, TX, pp. 785–809.

Moore, T.C., Shackleton, N.J., Pisias, N.G., 1993. Paleoceanography and diachrony of radiolarian events in the eastern equatorial Pacific. Paleoceanography 8, 567–586.

Morley, J.J., Shackleton, N.J., 1978. Extension of the radiolarian *Stylatractus universus* as a biostratigraphic datum in the Indian Ocean. Geology 6, 309–311.

Opdyke, N.D., Glass, B., Hays, J.D., Foster, J., 1966. Paleomagnetic study of Antarctic deep-sea cores. Science 154, 349–357.

Sakai, H., Keating, B., 1991. Paleomagnetism of Leg 119 – Holes 737A, 738C, 742A, 745B, and 746A. In: Wise, S.W., Jr., Schlich, R. et al. (Eds.), Proc. ODP Sci. Results 120. ODP, College Station, TX, pp. 751–770.

Shackleton, N.J., Berger, A., Peltier, W.R., 1990. An alternative astronomical calibration of the lower Pleistocene timescale based on ODP Site 677. Trans. R. Soc. Edinb. Earth Sci. 81, 251–261.

Shipboard Scientific Party, 1999. Site 1089. In: Gersonde, R., Hodell, D.A., Blum, P. et al. (Eds.), Proc. ODP Init. Rep. 177, pp. 1–97 [CD-ROM]. Available from: Ocean Drilling Program, Texas A&M University, College Station, TX.

Shipboard Scientific Party, 1999. Site 1091. In: Gersonde, R., Hodell, D.A., Blum, P. et al. (Eds.), Proc. ODP Init. Rep. 177, pp. 1–84 [CD-ROM]. Available from: Ocean Drilling Program, Texas A&M University, College Station, TX.

Shipboard Scientific Party, 1999. Site 1093. In: Gersonde, R., Hodell, D.A., Blum, P. et al. (Eds.), Proc. ODP Init. Rep. 177, pp. 1–104 [CD-ROM]. Available from: Ocean Drilling Program, Texas A&M University, College Station, TX.

Shipboard Scientific Party, 1999. Site 1094. In: Gersonde, R., Hodell, D.A., Blum, P. et al. (Eds.), Proc. ODP Init. Rep. 177, pp. 1–73 [CD-ROM]. Available from: Ocean Drilling Program, Texas A&M University, College Station, TX.

Spiess, V., 1990. Cenozoic magnetostratigraphy of Leg 113 drill sites, Maud Rise, Weddell Sea, Antarctica. In: Barker, P.F., Kennett, J.P. et al. (Eds.), Proc. ODP Sci. Results 113. ODP, College Station, TX, pp. 261–315.

Tucholke, B.E., Embley, R.W., 1984. Cenozoic regional erosion of the abyssal seafloor off South Africa. In: Schlee, J.S. (Ed.), Interregional Unconformities and Hydrocarbon Accumulation. Am. Assoc. Pet. Geol. Mem. 36, 145–164.

Zielinski, U., Gersonde, R., 2002. Plio-Pleistocene diatom biostratigraphy from ODP Leg 177, Atlantic sector of the Southern Ocean. Mar. Micropaleontol. 45, S0377-8398(02)00031-2.